J Therm Anal Calorim (2011) 105:113–122
DOI 10.1007/s10973-011-1445-5

Kinetic analysis of γ-MnO_2 thermal treatment

Wesley M. Dose · Scott W. Donne

Received: 11 October 2010 / Accepted: 7 March 2011 / Published online: 24 March 2011

Abstract Kinetic analysis of the thermal processes occurring during water loss for γ-MnO_2 was performed using two techniques, namely, the induction period and iso-conversional methods. The modelling and analysis arising from thermogravimetric studies of the material gave rise to the pre-exponential factor and, most importantly, the activation energy for the transition. Analysis using the induction period showed the activation energy to increase linearly with extent of conversion, ranging from 109–250 kJ mol^{-1}, while the iso-conversional method gave values in the range 66–76 kJ mol^{-1}, with higher values for both lower and higher extents of conversion. Comparison of these methods indicates that the iso-conversional method is the preferred technique for determining the kinetic parameters for this process. Overall, this allows for the determination of the optimum heat treatment temperature and time for the γ-MnO_2.

Keywords Manganese dioxide · Thermogravimetric analysis · Iso-conversional method · Induction period

Introduction

General

The worldwide market for portable consumer batteries is in excess of $US10 billion per annum, according to the General Manager of Eveready Battery Company, Inc. Systems using the manganese dioxide cathode make up the majority of this market due primarily to the excellent electrochemical properties of the manganese dioxide cathode. As electronic device technology advances, the demands placed on the batteries used to power them is increasing at a similar rate, thus shortening their life expectancy. To keep pace with these advances, there is a corresponding need to improve battery performance. The overall focus of this work is on the performance of the manganese dioxide cathode used in non-aqueous Li/MnO_2 cells where the complex interplay between structural properties and electrochemical behaviour is relatively unknown.

W. M. Dose · S. W. Donne (✉)
Discipline of Chemistry, University of Newcastle, Callaghan, NSW 2308, Australia
e-mail: scott.donne@newcastle.edu.au

Structural varieties

As a compound, manganese dioxide has a wide array of different crystal structures, so much so that over 30 different species have been classified [1, 2]. The importance of structure is that it determines the electrochemical behaviour of the material. It is therefore essential that we describe in some detail the structures we will encounter in this work.

Manganese in oxidation states II, III, and IV prefers almost exclusively an octahedral coordination, albeit somewhat distorted [3]. This is particularly true for Mn(III) containing species, since it is a Jahn–Teller distorted ion. Therefore, the basic building block for the majority of manganese oxides and hydroxides is the $[Mn(O^{2-}, OH^{-}, OH_2)_6]^{z+}$ octahedral unit [4]. Various corner and/or edge sharing assemblages of these octahedral units give rise to different structures [1, 2]. An alternative approach to interpreting manganese oxide structures is to visualise a hexagonal close-packed array of oxide anions, into which manganese cations are placed selectively into the octahedral sites.

The simplest manganese dioxide structure is that of β-MnO_2 (pyrolusite) which consists of corner sharing octahedra in the *a*–*b* plane, and edge sharing octahedra in the *c* direction. The result is a [1 × 1] tunnel structure progressing in the *c* direction, as shown in Fig. 1a. For this tetragonal structure, the unit cell parameters are $a_0 = 0.439$ nm and $c_0 = 0.287$ nm [1, 2]. In a similar way, the structure of ramsdellite can be visualised, this time though with both edge and corner sharing in the *a*–*b* plane to form a [2 × 1] tunnel headed into the *c* direction. Ramsdellite has an orthorhombic unit cell with $a_0 = 0.446$ nm, $b_0 = 0.932$ nm, and $c_0 = 0.285$ nm [1, 2]. A schematic of its structure is shown in Fig. 1b.

One of the more common forms of manganese dioxide is γ-MnO_2, which is the preferred phase for use in the alkaline manganese dioxide cathode [4], as well as being the precursor that is heat treated before being used in the non-aqueous Li/MnO_2 system. The basis for describing the γ-MnO_2 structure is as a random microscopic intergrowth between both the pyrolusite and ramsdellite structures of manganese dioxide [5], as shown in Fig. 1c. Other features associated with the γ-MnO_2 structure include cation vacancies, lower valent manganese cations (Mn(III)), and structural water present as protons associated with oxide anions so as to compensate for the charge deficiency incurred by cation vacancies and Mn(III) ions [6–9]. As a result, the chemical composition of γ-MnO_2 has been described as:

$$\left(Mn^{4+}\right)_{1-x-y}\cdot(\square)_x\cdot\left(Mn^{3+}\right)_y\cdot\left(O^{2-}\right)_{2-4x-y}\cdot\left(OH^-\right)_{4x+y} \quad (1)$$

where *x* and *y* represent the mole fraction of cation vacancies (□) and Mn(III) ions, respectively. Typical ranges for *x* and *y* in an unreduced γ-MnO_2 sample are 0.06–0.08 and 0.04–0.12, respectively [10]. Another structural component of γ-MnO_2 that has been proposed is microtwinning in the (021) and (061) growth planes [9]. Structural modelling including microtwinning has been used to explain the appearance of certain features in the X-ray diffraction pattern of γ-MnO_2; however, there is conflicting physical evidence as to its actual existence [11].

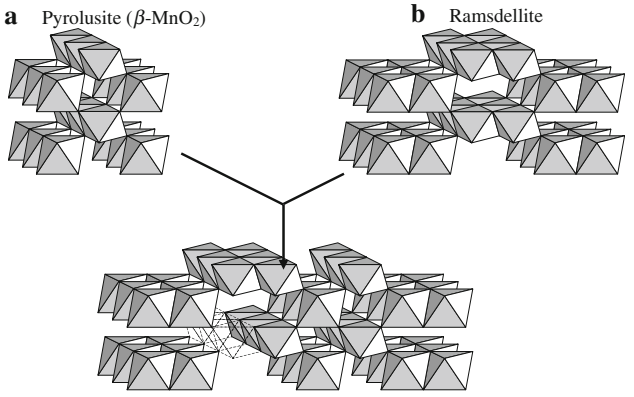

Fig. 1 Basic building blocks of the γ-MnO_2 structure in which **a** pyrolusite (β-MnO_2) and **b** ramsdellite have been microscopically intergrown to produce **c** γ-MnO_2

Clearly, based on the currently accepted structural and chemical (Eq. 1) definition, there can be a multitude of materials loosely classified as γ-MnO_2, even though their structural, and to some extent chemical, composition can vary considerably. There are many synthetic routes leading to γ-MnO_2, each with their own list of experimental variables that can alter its structural and chemical composition as defined above. However, the γ-MnO_2 used as the cathode-active material and as a precursor is most often prepared via electrolysis (electrolytic manganese dioxide, EMD) [4], which in itself imparts a unique morphology to the material. The original high resolution TEM work on γ-MnO_2 was conducted by Turner and Buseck [12], and it showed definitive evidence in support of De Wolff's microscopic intergrowth model for γ-MnO_2 [5]. More recent TEM work on γ-MnO_2 by Heuer et al. [11] has shown the material to consist of needle-like crystallites $\sim 10 \times 10 \times 100$ nm in size. These needles were then found to be assembled in a somewhat ordered fashion into grains ~ 200 nm in diameter. These grains were then found to be arranged randomly to form the bulk structure. Also apparent between the crystallites and grains were pores, into which electrolyte is expected to permeate during electrochemical discharge.

Heat treatment of γ-MnO_2

Before use as the active material in a non-aqueous Li/MnO_2 cell, the γ-MnO_2 precursor must be heat treated to remove water that would otherwise be extracted from the manganese dioxide during immersion in the non-aqueous media, and hence react with the metallic lithium anode causing a decrease in overall battery performance. Various stages in the heat treatment of γ-MnO_2 have been documented in the literature, and can be summarised as follows [13]:

$$\gamma\text{-}MnO_2 \xrightarrow{I} \beta\text{-}MnO_2 \xrightarrow{II} Mn_2O_3 \xrightarrow{III} Mn_3O_4 \xrightarrow{IV} MnO \quad (2)$$

Step I corresponds to the loss of water, as well as to a structural transition from the intergrowth γ-MnO_2 phase to the thermodynamically favoured β-MnO_2 phase. Three classes of water have been identified previously using thermogravimetric (TG) analysis, i.e. Type 1 water, which is physisorbed water able to be reversibly removed around 100 °C; Type 2 water, which is comprised of surface bound hydroxyls and water of crystallization that is irreversibly

removed around 200 °C; and Type 3 water, which are bulk hydroxyl groups removed irreversibly at 300 °C [14, 15]. Above 400 °C, thermal reduction takes place [16], with Step II occurring in the range 460–570 °C, Step III in the range 700–800 °C, and Step IV above 1300 °C. The mechanism for these transitions in the thermal treatment is known to be a function of the origin and history of the starting material, as well as the environment in which the heat treatment is carried out [16–21]. For instance, if Step I is carried out in an oxygen containing atmosphere, then oxidation of any Mn(III) present (Eq. 1) will also occur in addition to water loss and the structural transition.

As a final comment, it is Step I that is of most interest to the battery industry, i.e. heat treatment up to 400 °C. Removal of water is of primary importance, and as a consequence the structural transition to β-MnO_2 also occurs. However, so as to retain electrochemical capacity from the Mn(IV) species, the heat treatment must not be so intense as to lower the oxidation state of the active material, i.e. progress to Step II, III, or IV.

This work

The overall objective of this work is to improve the performance of manganese dioxide as the cathode material in a non-aqueous Li/MnO_2 cell. Since the γ-MnO_2 precursor must be heat treated prior to use to remove water, there is considerable scope for optimising its performance by examining the influence of the starting material structure and morphology, as well as the heat treatment temperature and duration. This relationship is at present poorly understood. However, more fundamental than this is examining the kinetics of the water loss and structural transition processes in Step I. As such, what we report here is our work on extracting kinetic information from thermogravimetric data as a means of characterising Step I in the heat treatment process.

Experimental

Starting material

The sample of γ-MnO_2 used in this work was prepared by anodic electrodeposition, and hence given the designation electrolytic manganese dioxide, or EMD. The cell used for electrolysis was based on a temperature controlled 2 L glass beaker in which two 144 cm^2 (72 cm^2 on either side) titanium sheets were used as the anode substrate, and three similarly sized copper sheets were used as the cathode substrate. The electrodes were arranged alternately so that each anode was surrounded on both sides by a cathode. The electrolyte was an aqueous mixture of $MnSO_4$ (1 M) and H_2SO_4 (0.25 M) maintained at 97 °C. Electrodeposition of the manganese dioxide was conducted with an anodic current density of 65 $A\ m^{-2}$ according to the reactions

$$\text{Anode (Ti): } Mn^{2+} + 2H_2O \rightarrow MnO_2 + 4H^+ + 2e^- \quad (3)$$

$$\text{Cathode (Cu): } 2H^+ + 2e^- \rightarrow H_2 \quad (4)$$

$$\text{Overall: } Mn^{2+} + 2H_2O \rightarrow MnO_2 + 2H^+ + H_2 \quad (5)$$

The overall process was carried out for 3 days, during which time the electrolyte Mn^{2+} concentration was of course depleted, while the H^+ concentration increased. To counteract this, and hence maintain a constant electrolyte concentration over the duration of the deposition, a concentrated (1.5 M) $MnSO_4$ solution was added continually at a suitable rate to replenish Mn^{2+} and dilute any excess H_2SO_4 produced. Under these conditions, control of the solution conditions was typically maintained to within ±2%.

After deposition was complete, the solid γ-MnO_2 deposit was mechanically removed from the anode and broken into chunks ~0.5 cm in diameter, and then immersed in 500-mL DI water to assist in the removal of entrained plating electrolyte. The pH of this chunk suspension was adjusted to pH 7 with the addition of 0.1 M NaOH. After ~24 h at a pH of 7, the suspension was filtered and the chunks then dried at 110 °C. After drying, the chunks were then milled to a −105 μm powder (mean particle size ~45 μm) using an orbital zirconia mill. The powder was then suspended in ~500 mL of DI water, and its pH again adjusted to 7 with the further addition of 0.1 M NaOH. When the pH had stabilized, the suspension was filtered and the collected solids dried at 110 °C. When dry the powdered γ-MnO_2 was removed from the oven, allowed to cool to ambient temperature in a dessicator and then transferred to an airtight container for storage.

The structure of this material was confirmed to be γ-MnO_2 using a Phillips PW1710 diffractometer employing Cu Kα radiation (Fig. 2). The BET surface area [22] of this material (after de-gassing under vacuum at 110 °C for 2 h) was measured using N_2 gas adsorption at 77 K and found to be 57.9 $m^2\ g^{-1}$.

Thermogravimetric (TG) analysis

TG analysis was conducted using a Perkin Elmer Diamond TG/DTG controlled by Pyris software. Approximately, 10 mg of γ-MnO_2 sample was added to an aluminium sample pan and placed into the analyser. The same mass of α-Al_2O_3 in a similar aluminium pan was used as the reference material for DTA measurements. With the sample and reference materials loaded, and the furnace closed, dry nitrogen gas was passed over the sample at 20 mL min^{-1} for 30 min prior and during the heating profile. The heating

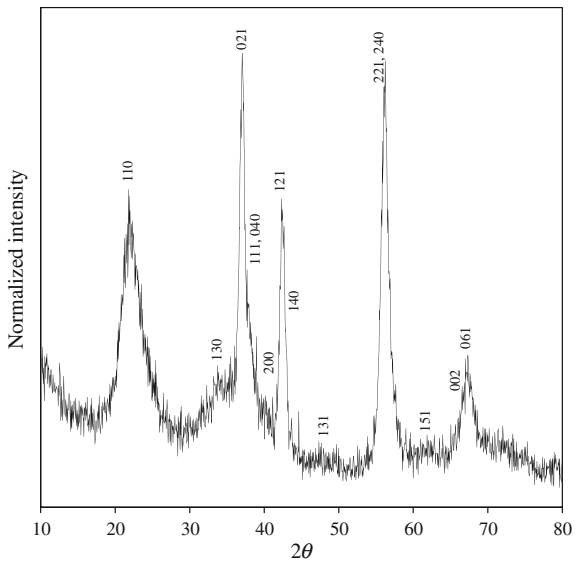

Fig. 2 XRD pattern of the γ-MnO_2 used in this work showing the γ-MnO_2 structure, with the corresponding Miller indices indexed using an orthorhombic unit cell

profile applied to the sample was essentially a linear ramp at rates ranging from 0.25–10 °C min^{-1}.

Results and discussion

Thermogravimetric analysis

The thermogravimetric (TG) and differential thermogravimetric (DTG) data for the thermal decomposition of γ-MnO_2 at the various heating rates are shown in Figs. 3 and 4, respectively. The initial loss in mass up to ~120 °C is due to the removal of physisorbed water from the γ-MnO_2 surface. Manganese oxides are well known for their ability to adsorb water [23], so it is not surprising that 2–3% of the initial sample mass is physisorbed water. The broad peak at ~200 °C in the DTG relates to the removal of structural water, i.e. protons associated with cation vacancies and Mn(III) ions within the manganese dioxide structure. The sharper peak at ~500 °C relates to Step II corresponding to thermal reduction of the MnO_2 to form Mn_2O_3. The use of faster heating rates has shifted the decomposition temperature to higher values possibly as a result of slow reaction kinetics and/or since less time is allowed for the equivalent reaction. It is also possible that the thermal conductivity of the γ-MnO_2 contributed to this effect, although with the use of a relatively small sample size (10 mg) its contribution is expected to be minor.

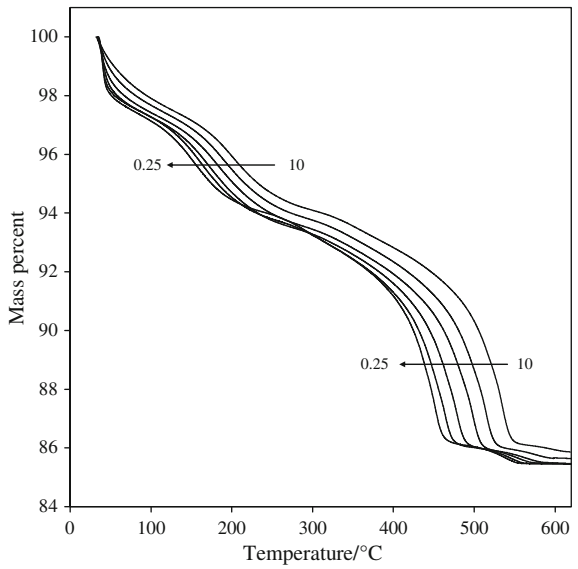

Fig. 3 TG data for the γ-MnO_2 sample used in this work recorded at rates of 0.25, 0.5, 1.0, 2.5, 5.0, and 10.0 °C min^{-1}

Multiple curve isoconversional analysis

In this analysis, we will be considering Step I of the γ-MnO_2 thermal decomposition; i.e. the process of removing water from the structure beginning at ~175 °C, since this is most important when the material is to be used in a non-aqueous battery system.

The first step in the analysis was background correction of the DTG data. To do this an exponential background

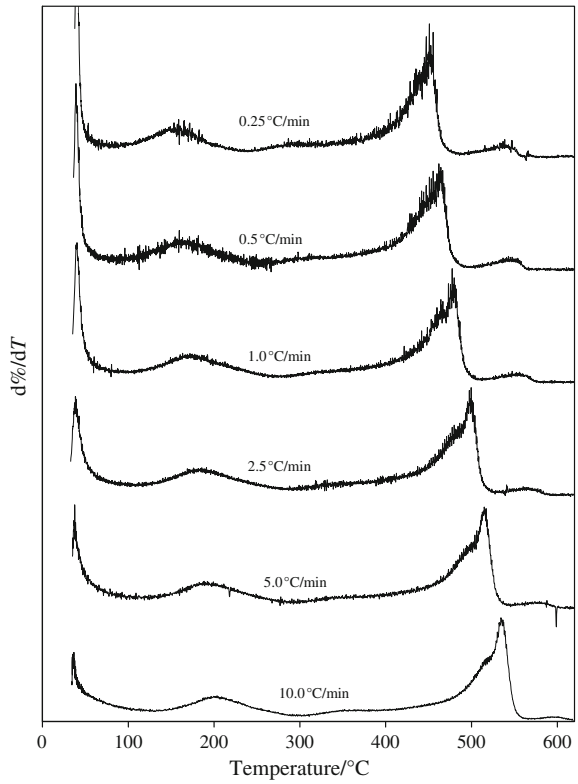

Fig. 4 Differential thermogram (DTG) for the γ-MnO_2 sample heated at different heating rates

curve was fitted to the data surrounding the peak for each heating rate used. The resulting curve after background correction describes the processes occurring in this region, as shown in Fig. 5 for a heating rate of 10 °C min^{-1}. The normalised extent of conversion (α) was then found by numerical integration of the background-corrected DTG data, with the normalisation being carried out by expressing each point relative to the maximum area determined. A plot of α as a function of temperature for the range of heating rates considered is shown in Fig. 6. From this data, the temperatures corresponding to a pre-defined set of α values can be found for each heating rate, as shown in Fig. 7.

Kinetic analysis using this method is conventionally applied to the data corresponding to $\alpha = 0$ for the different heating rates. However, since we have access here to the temperature corresponding to various extents of conversion for different heating rates, and the fact that we will apply the method used for $\alpha = 0$ to all α values, then it will be interesting to observe how the resultant kinetic parameters change. Kinetic analysis is based on the rate equation:

$$\beta\frac{d\alpha}{dT} = Af(\alpha)\exp\left(-\frac{E_A}{RT}\right) \tag{6}$$

where A is the pre-exponential factor (min^{-1}), β is the heating rate (°C min^{-1}), E_A is the activation energy (J mol^{-1}), the term $f(\alpha)$ represents the model chosen to represent the mechanism of thermal decomposition, and all other symbols have their usual significance. In this case, we will use $f(\alpha) = 1 - \alpha$ as our decomposition model [24]. Separation of variables leads to

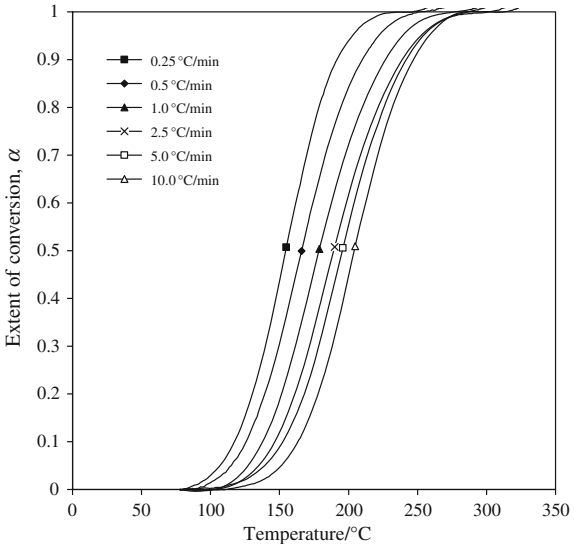

Fig. 6 Extent of conversion versus temperature for the different heating rates

$$\frac{d\alpha}{f(\alpha)} = \frac{A}{\beta}\exp\left(-\frac{E_A}{RT}\right)dT \tag{7}$$

and then integration of the left-hand side from 0 to α_i in Eq. 7, gives:

$$F(\alpha_i) - F(0) = \int_0^{T_i}\left(\frac{A}{\beta}\right)\exp\left(-\frac{E_A}{RT}\right)dT \tag{8}$$

where F represents the integrated form of $f(\alpha)$ and T_i corresponds to the temperature at α_i. Upon rearrangement, we can write:

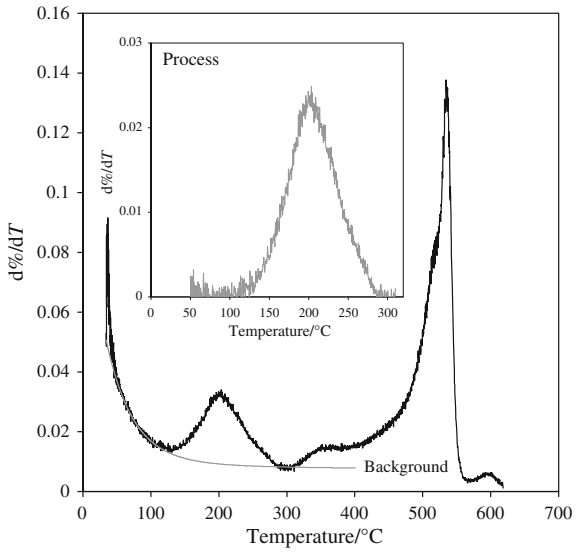

Fig. 5 Fitting of DTG data for heating rate 10 °C min^{-1} with background curve and resulting process

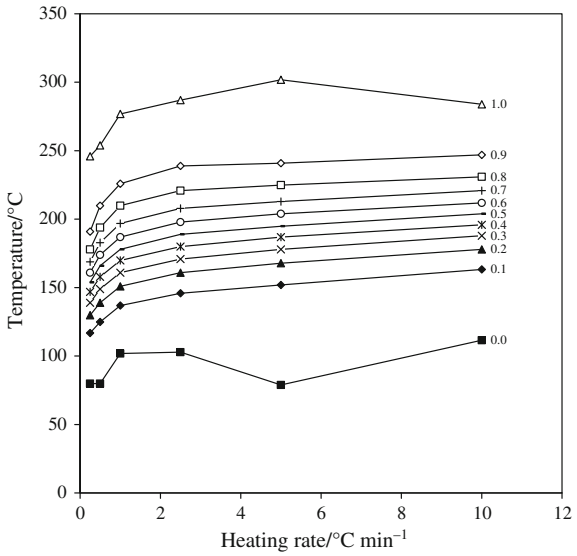

Fig. 7 Variation of temperature with heating rate for given extent of conversion

$$\beta = \int_0^{T_i} \left(\frac{A}{F(\alpha_i) - F(0)}\right) \exp\left(-\frac{E_A}{RT}\right) dT \quad (9)$$

This integration was performed numerically using the trapezium method and optimised to fit the experimental data using a linear least squares regression. Consequently, the dependence of activation energy on the extent of conversion and the pre-exponential factor was found, as shown in Fig. 8. With the exception of the first point at $\alpha = 0$ (which was likely due to the noisy data for these conditions, cf. Fig. 7), the activation energy clearly increases with extent of conversion, ranging from 109-250 kJ mol^{-1}.

Before going further, an additional comment needs to be made regarding the choice of thermal decomposition model (f(α)) used in the analysis. Each of the models listed in Ref. [24] were examined here using this approach. Firstly, despite the broad range of curve shapes (α vs. *T*) that these models generate, no single one was able to fit satisfactorily to the experimental data, hence the use of the incremental approach in our analysis. As we will discuss later, this provides strong supporting evidence for multiple mass loss processes occurring. In addition, with the application of the incremental approach, it was noted that for each thermal decomposition function ($f(\alpha)$) used the measured activation energy was similar to that reported in Fig. 8, with similar variation in the activation energy across the extent of conversion (α). Again, this suggests the presence of multiple mass loss processes, as well as provides us with some confidence for using the first-order $f(\alpha) = 1 - \alpha$ expression over the range used. Finally, the use of this model enables us to quite easily calculate the required isothermal time necessary to achieve a specified extent of conversion.

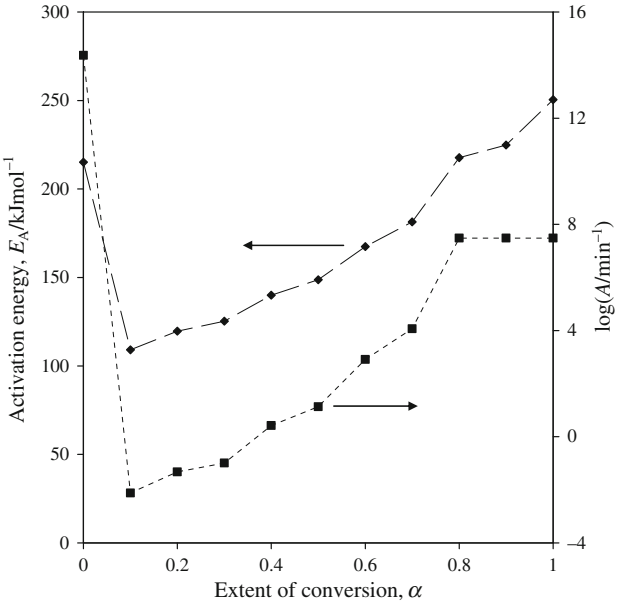

Fig. 8 Activation energy and pre-exponential factor for process occurring against extent of conversion calculated using the first order kinetic analysis

Single curve incremental isoconversional analysis

Another approach to solving the rate expression in Eq. 6 is the incremental integral method [24, 25]. This method can also be used to take into account the dependence of the kinetic parameters on the extent of conversion, focussing instead on an individual TG experiment rather than a range of different heating rate experiments. In this case, the Runge–Kutta method, an iterative technique for the approximation of ordinary differential equations, was used to solve Eq. 6. This method uses the previous point (α_n, T_n) to approximate the next (α_{n+1}, T_{n+1}), by using the size of the interval between the points (h) and an estimate average of the slopes. To begin we have the initial condition

$$\alpha(T_0) = \alpha_0 = 0 \quad (10)$$

Then, using the Runge–Kutta method, α_{n+1} and T_{n+1} are given by

$$\alpha_{n+1} = \alpha_n + \frac{1}{6}h(k_1 + 2k_2 + 2k_3 + k_4) \quad (11)$$

$$T_{n+1} = T_n + h \quad (12)$$

where h is the size of the interval (1 K was used in this analysis), and

$$k_1 = f(T_n, \alpha_n) \quad (13)$$

$$k_2 = f\left(T_n + \frac{h}{2}, \alpha_n + \frac{hk_1}{2}\right) \quad (14)$$

$$k_3 = f\left(T_n + \frac{h}{2}, \alpha_n + \frac{hk_2}{2}\right) \quad (15)$$

$$k_4 = f(T_n + h, \alpha_n + hk_3) \quad (16)$$

where the function $f(T,\alpha)$ is implied by Eq. 6. This gives rise to a theoretical curve for the extent of conversion against temperature, which can be fitted to the experimental curve using linear least squares regression in a restricted range of α (hence employing the incremental integral method), by varying values for the activation energy, E_A, and the pre-exponential factor, A. Figure 9 demonstrates how the activation energy changes as a function of extent of conversion and heating rate. Because the focus here is on just one data set, particular attention was paid to the fitting procedure to ensure that a global minimum was determined. This was achieved by repeating the fitting multiple times, from different starting points. In each case, across the complete α range and for each heating rate used, the same result was achieved.

The pre-exponential factor for all analyses remained essentially constant at a value of (5.3 ± 0.8) × 10^6 min^{-1},

where the error analysis here takes into account the variation in the calculated A value.

Overall, the calculated activation energy for the mass loss associated with the thermal decomposition of γ-MnO_2 fell within the rather narrow range 66–77 kJ mol^{-1}. Nevertheless, within this range, there were some systematic changes observed. For all heating rates there was a minimum, or for lower heating rates, a plateau in the activation energy within the extent of conversion range $0.1 < \alpha < 0.7$. At both higher and lower α values the activation energy increases. This increase is interesting in that it tells us something about the availability of energy or heat, as well as reactants, to affect the thermal transformation. At low α values, corresponding to lower temperatures, there is insufficient heat to activate the reaction, so, for all intents and purposes, the activation energy is much larger than normal because very little reaction is occurring. Conversely, at higher α values there is a relatively low concentration of unreacted species available to actually undergo the thermal transformation, and as such the rate of the thermal transformation here is also inhibited (manifested as an increase in activation energy), since reactant concentration is also a limiting factor in chemical reactions. What is also interesting about the data in Fig. 9 is the general decrease in calculated activation energy as the heating rate was increased. This is quite clearly demonstrated in Fig. 10, which shows how the activation energy at $\alpha = 0.5$ changes with heating rate. The data in this figure indicates that there are two heating rate regions for which there is an exponential decrease in calculated activation energy with heating rate. The cause of this may lie in the apparently less than ideal thermal transfer of heat from the furnace to the sample during the TG experiment. Whether there is a thermal gradient within the powdered sample in the TG pan, or within individual sample particles, it does mean that the thermal decomposition reaction will be occurring at different rates within the sample and/or individual particles. Certainly at higher heating rates this thermal gradient will be much more pronounced, meaning that there is expected to be a greater error in the estimated activation energy when determined at faster heating rates. While the thermal conductivity of manganese dioxide is, to the best of our knowledge, not available in the literature, other similar metal oxides have relatively high thermal conductivities, as shown in Table 1 [26]. Typical thermal conductivity values lie within the range 2–30 W m^{-1} K^{-1}. Of these, the value for titanium dioxide (3.8 W m^{-1} K^{-1}) is most likely very similar to manganese dioxide given the proximity of the metals to each other in the periodic table, and the iso-structural nature of the corresponding oxides. This relatively low value does imply that there will be a reasonable thermal gradient across each particle. To

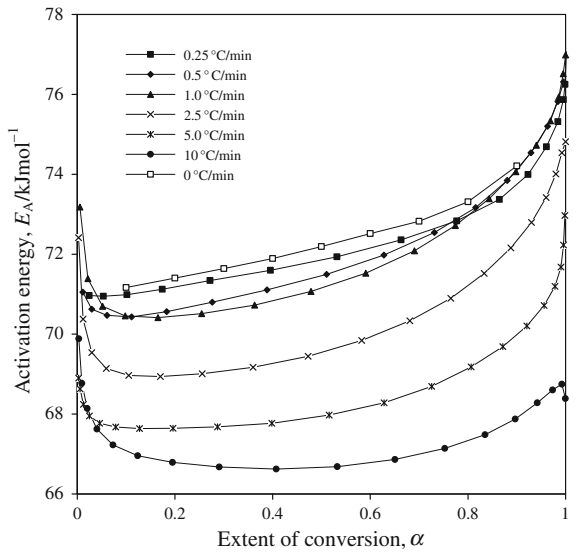

Fig. 9 Activation energy with respect to extent of conversion for the different heating rates

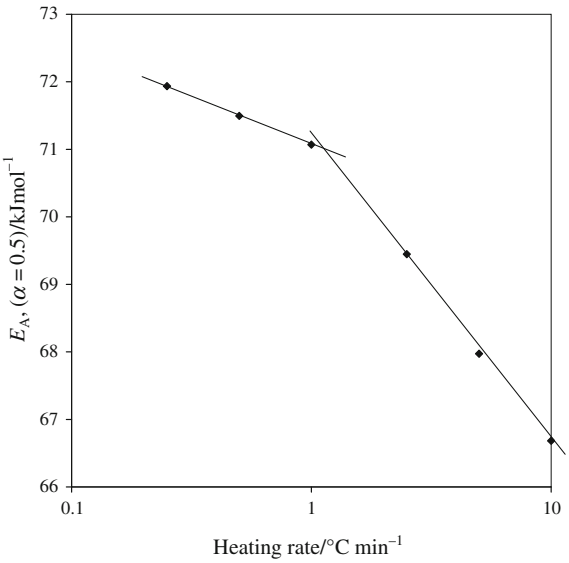

Fig. 10 Activation energy (for $\alpha = 0.5$) as a function of heating rate

Table 1 Thermal conductivity of selected metal oxides [26]

Metal oxide	Thermal conductivity/W m^{-1} K^{-1}
Al_2O_3 (sintered)	26 (373 K)
$BaTiO_3$	6.2 (300 K)
Fe_3O_4 (magnetite)	7.0 (304 K)
MnO	3.5 (573 K)
SiO_2 (fused silica)	1.6 (373 K)
$SrTiO_3$	11.2 (300 K)
TiO_2	3.8 (400 K)

Table 2 Isothermal heating regimes to achieve complete conversion of the water loss process

Temperature/°C	Heating time/h
200	31.65
250	11.12
300	5.07
350	1.52
400	0.27

eliminate the effect of thermal conductivity, the exponential relationship between heating rate and calculated activation energy was extrapolated to predict the activation energy under the hypothetical condition of a 0 °C min^{-1} heating rate. This extrapolated data is also shown in Fig. 9, and is expected to more closely represent the true activation energy for this thermal decomposition process.

As was mentioned previously, the systematic variation in the activation energy, as shown in Fig. 9 and highlighted specifically in Fig. 10 quite nicely validates the use of this method for the thermal analysis of kinetic parameters. The International Confederation for Thermal Analysis and Calorimetry (ICTAC) has recommended that single scan methods of analysis be avoided where possible (see for example [27]). However, in this work the activation energies obtained were not just based on one analysis. In fact, what we have shown here is that the systematic variation within the activation energy over two orders of magnitude change in heating rate (Fig. 10) not only provide us with considerable confidence in the resultant data, but also allows us to extrapolate to what the theoretical activation energy would be at a 0 °C min^{-1} heating rate. This latter outcome has not been reported previously, at least for this system, and in actual fact represents a novel approach to determining an activation energy that is free of experimental artefacts, such as thermal transfer of heat to the sample.

Finally, the kinetic parameters determined for the water loss process can be used to calculate the required isothermal time to achieve complete conversion of the material ($\alpha = 1$), i.e. completely remove water from the material, at a range of temperatures. This value can be found by employing the Arrhenius equation to calculate the rate constant (k) and subsequently, assuming first order kinetics, the heating time can be determined. This was performed for the heating rate 1 °C min^{-1}, and is shown in Table 2.

Comparison of methods

The first order analysis of the kinetics has shown that the activation energy for the loss of water from the manganese dioxide structure increased relatively linearly with extent of conversion, varying from $\sim$109 kJ mol^{-1} at $\alpha = 0.1$ to $\sim$250 kJ mol^{-1} at $\alpha = 1.0$. On the other hand, the incremental integral method led to an activation energy of 66–76 kJ mol^{-1} throughout the majority of the thermal transformation, with slightly higher values at both lower and higher extents of the conversion. Clearly, there are significant differences in the results obtained from the application of the two kinetic analysis methods, and these differences need to be addressed.

From a purely statistical perspective, the use of multiple experiments to produce data for analysis is bound to contain more variation than just using a single experiment. Under these circumstances, therefore, we might expect that the incremental integral approach should inherently be more reliable than the first-order analysis method. Nevertheless, the contribution to the total variation in the analysis made by the individual TG experiments is expected to be quite small, certainly not enough to account for the significant difference between the two methods.

As part of the analysis a background correction of the DTG data was employed to focus specifically on the mass loss process of interest, i.e. the loss of structural water from the manganese dioxide. While this background correction was applied to all of the data reported here, it was in no way constant between experiments. Furthermore, the shape of the background correction curve was arbitrarily chosen to be exponential. The point being made is that the background correction being made could have easily over- or under-compensated its contribution to the total response, thus inducing some variability between experiments. This would certainly suggest that the incremental integral approach should be the preferred method.

Another likely contributor to variability in the analysis is the thermal conductivity of the manganese dioxide in relation to the heating rate used. Despite the fact that only a small quantity of material ($\sim$10 mg) was used in each experiment, the rate with which heat is transferred through the sample is very critical in determining the validity of the resultant information, particularly so since the kinetic analysis model assumes that the sample temperature is uniform throughout. As has already been mentioned, the thermal conductivity of manganese dioxide is not available in the literature, however, the thermal conductivity of similar materials (e.g. titanium dioxide) does suggest that there may be thermal gradients within the manganese dioxide, particularly with the use of fast heating rates. Therefore, those experiments that make use of the higher heating rates could be judged as having a higher relative error compared to those using slower heating rates. Therefore, the incremental integral approach, particularly for those experiments employing a slower heating rate, is most likely to be the preferred method.

As a final comment, the first-order kinetic analysis involved the use of separation of variables to solve Eq. 6.

An inherent assumption made with this approach is that the extent of conversion is independent of temperature, when in fact this is not the case given the thermal gradients within the manganese dioxide sample and the fact that the conversion process we are examining covers a very broad temperature range. Under these circumstances, while the data we have collected shows a very nice asymptotic change with heating rate (Fig. 10), the assumptions made in the numerical analysis does not lead to an accurate estimate of the activation energy, again implying that the incremental integral approach is superior.

Summary and conclusions

We have used a first-order kinetic analysis method and an incremental integral approach to perform kinetic analysis on the water loss of manganese dioxide, determining the pre-exponential factor and the activation energy for this process. Thermogravimetric experiments were performed on the γ-MnO_2 at different scan rates and this data formed the basis for our analysis of Step I (Eq. 2) in the thermal treatment of manganese dioxide. Both methods used found the activation energy as a function of the extent of conversion, hence allowing for variation in the values over the process studied, while the incremental integral method also varied with heating rate.

The first order kinetic analysis method gave the activation energy to increase relatively lineally with extent of conversion from $\sim$109–250 kJ mol^{-1}. Contrary to this, using the incremental integral method, the activation energy was found to lie in the range of 66–76 kJ mol^{-1}, with higher values at both lower and higher extents of conversion. This result indicated the influence of both the availability of energy or heat and the reactants on the thermal transformation of γ-MnO_2. A comparison and investigation into the significant differences found using these two methods indicate that the incremental integral method is the preferred means for obtaining the kinetic parameters describing this process. This result stems back to the use of a single TG experiment and the exclusive use of a slower scan rate using the incremental integral method (multiple scan rates, and thus experiments, are required in the first order kinetic analysis method). A single experiment avoids inherent variability between multiple experiments and limits errors induced in the somewhat arbitrary application of the background correction. Using slower scan rates reduces the possible undesired effects arising from thermal gradients across the sample as a result of the thermal conductivity of the material.

In conclusion, this work demonstrates two methods for obtaining the kinetic parameters describing the water loss as a result of thermal heat treatment of γ-MnO_2. This knowledge provides further insight into the processes occurring during the heat treatment, which in turn will lead to a better understanding of the optimal heat treatment regime for γ-MnO_2, and hence a better performing material for use in non-aqueous batteries.

References

1. Burns RG, Burns VM. Structural relationships between the manganese(IV) oxides. Proc MnO2 Symp. 1975;1:306–27.
2. Burns VM, Burns RG, Zwicker WK. Classification of natural manganese dioxide minerals. Proc MnO2 Symp. 1975;1:288–305.
3. Giovanoli R. On natural and synthetic manganese nodules. In: Varentsov IM, Grasselly G, editors. Geology and geochemistry of manganese. Budapest: Akademiai Keadó; 1980. p. 159–202.
4. Ward CB, Walker AI, Taylor AR. The production of alkaline grade EMD at Australian Manganese Company Limited. Prog Batt Batt Mater. 1992;11:40–6.
5. De Wolff PM. Interpretation of some γ-MnO_2 diffraction patterns. Acta Cryst. 1959;12:341–5.
6. Ruetschi P. Cation-vacancy model for manganese dioxide. J Electrochem Soc. 1984;131:2737–44.
7. Ruetschi P. Influence of cation vacancies on the electrode potential of manganese dioxide. J Electrochem Soc. 1988;135:2657–63.
8. Ruetschi P, Giovanoli R. Cation vacancies in manganese dioxide and their influence on electrochemical reactivity. J Electrochem Soc. 1988;135:2663–9.
9. Chabre Y, Pannetier J. Structural and electrochemical properties of the proton/γ-MnO_2 system. Prog Solid State Chem. 1995;23:1–130.
10. Williams RP. Characterisation and production of high performance electrolytic manganese dioxide for use in primary alkaline cells. PhD Thesis, University of Newcastle, Australia; 1995.
11. Kim C, Akase Z, Zhang L, Heuer AH, Newman AE, Hughes PJ. The structure and ordering of ε-MnO_2. J Solid State Chem. 2006;179:753–74.
12. Turner S, Buseck PR. Manganese oxide tunnel structures and their intergrowths. Science. 1979;2003:456–8.
13. Liu B, Thomas PS, Ray S, Williams RP. The effect of sampling conditions on the thermal decomposition of electrolytic manganese dioxide. J Therm Anal Calorim. 2004;76:115–22.
14. Lee JA, Newnham CE, Tye FL. Energetics of water desorption from a γ-manganese dioxide. J Colloid Interface Sci. 1973;42:372–80.
15. Lee JA, Newnham CE, Tye FL. Thermal behavior of gamma-manganese dioxide and some reduced forms in oxygen. J Chem Soc Faraday Trans. 1978;74:237–49.
16. Desai BD, Fernandes JB, Dalal VNK. Manganese dioxide—a review of a battery chemical. Part II. Solid state and electrochemical properties of manganese dioxides. J Power Sources. 1985;16:1–43.
17. Skidmore PR. A thermal analysis study of IBA samples. Prog Batt Solar Cells. 1990;9:167–70.
18. Zaki MI, Hasan MA, Pasupulety L, Kumari K. Thermochemistry of manganese oxides in reactive gas atmospheres: Probing redox compositions in the decomposition course $MnO_2 \rightarrow MnO$. Thermochim Acta. 1997;303:171–81.
19. Giovanoli R. Thermogravimetry of manganese dioxides. Thermochim Acta. 1994;234:303–13.
20. Gonzalez C, Gutierrez JI, Gonzales-Velasco JR, Arranz A, Arranz JF. Application of differential scanning calorimetry to the

reduction of several manganese oxides. J Therm Anal Calorim. 1998;52:985–9.
21. El-Shobaky A, Ghozza AM, Hassan HA. Thermal decomposition of manganese carbonate supported on active alumina. J Therm Anal Calorim. 1998;51:529–39.
22. Brunauer S, Emmett PH, Teller E. Adsorption of gases in multimolecular layers. J Am Chem Soc. 1938;60:309–19.
23. Fraioli AV. Investigation of manganese dioxide as an improved solid desiccant. Proc Electrochem Soc. 1985;85–4:342–68.
24. Budrugeac P, Segal E. Some methodological problems concerning nonisothermal kinetic analysis of heterogeneous solid-gas reactions. Int J Chem Kinet. 2001;33:564–73.
25. Simon P, Thomas PS, Okiliar J, Ray AS. An incremental integral isoconversional method. J Therm Anal Calorim. 2003;72:867–74.
26. Haynes WM, editor. CRC handbook of physics and chemistry. 91st ed. USA: CRC Press; 2009.
27. Maciejewski M. Computational aspects of kinetic analysis. Part B: the ICTAC Kinetics Project B—the decomposition kinetics of calcium carbonate revisited, or some tips on survival in the kinetic minefield. Thermochim Acta. 2000;355:145–54.